Correlated light and electron microscopy: ultrastructure lights up!

Pascal de Boer[1], Jacob P Hoogenboom[2] & Ben N G Giepmans[1]

Microscopy has gone hand in hand with the study of living systems since van Leeuwenhoek observed living microorganisms and cells in 1674 using his light microscope. A spectrum of dyes and probes now enable the localization of molecules of interest within living cells by fluorescence microscopy. With electron microscopy (EM), cellular ultrastructure has been revealed. Bridging these two modalities, correlated light microscopy and EM (CLEM) opens new avenues. Studies of protein dynamics with fluorescent proteins (FPs), which leave the investigator 'in the dark' concerning cellular context, can be followed by EM examination. Rare events can be preselected at the light microscopy level before EM analysis. Ongoing development—including of dedicated probes, integrated microscopes, large-scale and three-dimensional EM and super-resolution fluorescence microscopy—now paves the way for broad CLEM implementation in biology.

© 2015 Nature America, Inc. All rights reserved.

Fluorescence microscopy (FM) allows researchers to identify specific molecules and study their biological roles. However, because a large fraction of molecules remain unlabeled and therefore 'in the dark', the context of the localization is lost. In addition, the resolution of light microscopy (LM) is typically submicrometer and thus does not match the size of biomolecules, which typically range from 0.1 to 10 nm. The way to analyze molecules both in their biological context and at high resolution is via EM. However, with EM, ultrastructural analysis is on grayscale images, in which molecules are hard to define; biological samples are in a fixed state; and finding rare events in space and time is nearly impossible. These limitations can be overcome with CLEM (**Box 1**), which combines the strengths of the two modalities and enables the analysis of rare cellular (or subcellular) events in their cellular context. Recent developments in probes, sample preparation, super-resolution FM, image overlay, dedicated microscopes and data handling have provided a boost for CLEM in the past decade. Not only is resolution now better matched between the two modalities but EM analysis can now also be performed over larger volumes. Together with improving methodology, better matched scales (**Fig. 1**) between the two modalities makes CLEM more widely applicable in biology. Here we review the basic ingredients for CLEM, as well as the latest developments. We provide guidelines, tips and tricks for their generic implementation in biology, and we discuss the road ahead toward crisp and bright CLEM analysis of cells, structures, molecules and ultrastructure.

MICROSCOPY AND ACQUISITION

CLEM is typically performed in one of two ways in which any FM or EM modality can be used: (i) samples are analyzed by fluorescence imaging—for instance, time-lapse studies of FP-tagged proteins—followed by fixation and further EM processing, acquisition and analysis, or (ii) ultrathin sections prepared for EM still contain fluorescent label, or are fluorescently labeled, and are imaged with both LM and EM (**Fig. 2**), for instance after immunolabeling. The latter approach also allows for analysis with integrated microscopes as discussed below. Probes to identify specific molecules, organelles or cells are either genetically encoded or affinity based.

[1]Department of Cell Biology, University Medical Center Groningen, University of Groningen, Groningen, the Netherlands. [2]Faculty of Applied Sciences, Delft University of Technology, Delft, the Netherlands. Correspondence should be addressed to B.N.G.G. (b.n.g.giepmans@umcg.nl) or J.P.H. (j.p.hoogenboom@tudelft.nl).

RECEIVED 27 AUGUST 2014; ACCEPTED 15 APRIL 2015; PUBLISHED ONLINE 28 MAY 2015; DOI:10.1038/NMETH.3400

BOX 1 CLEM TERMINOLOGY

CLEM is the acronym for correlated (or correlative) light microscopy and electron microscopy, where light microscopy typically refers to fluorescence light microscopy. CLEM implementation varies widely and is often based on the hardware used. Examples of hardware include ILEM[32] and SCLEM[15] for integrated microscopes and simultaneous CLEM, respectively. However, the "I" in ILEM may refer to immunobased CLEM, and the "S" in SCLEM to scanning or serial CLEM. Moreover, in "cryo-CLEM," the term "cryo" may refer to cryo-EM with cryo-LM or with room-temperature FM. We propose to use the acronym CLEM generally, with further explanation detailed in materials and methods sections of research articles.

A subset of specific CLEM probes can allow detection in both microscopes. However, precautions or specific strategies are needed to perform CLEM: routine FM procedures and EM preparation are often mutually exclusive in that either fluorescence is lost or the ultrastructure is destroyed. Thus, CLEM requires special attention to sample preparation[1].

Sample preparation

Chemical fixation and embedding. Classical EM preparation involves fixation and staining with heavy metals followed by plastic embedding and sectioning[2,3] (**Figs. 2a–c** and **3**). Labeled molecules may be visualized after EM preparation using sequential FM and EM contrast with combinatorial tags (**Figs. 2a–c** and **3**) or post-embedding labeling of the section (discussed below in Probes for CLEM). Common fluorescent probes, such as FPs, are incompatible with classical EM sample preparation; although protocols can be used to preserve fluorescence in the EM sample, for both immunotargeted fluorophores[4,5] and genetically encoded probes[6–11] (**Fig. 2d,e**), this may come at the expense of ultrastructural preservation. Fluorescence reduction caused by treatment with high concentrations of osmium and by complete dehydration may be prevented by cryofixation[6,7,10,12] or Tokuyasu-like sample preparation[13]. Integrated FM-EM inspection in a vacuum is also being optimized[10,14,15] (**Fig. 2d,e**). Alternatively, cryogenic EM can be performed.

Cryo-microscopy. In cryo-electron microscopy (cryo-EM), biomaterials are preserved in a near-native frozen hydrated state, which does not require chemical fixation or embedding. Samples (small cells, viruses or macromolecules) can be rapidly vitrified, which allows for fluorescence preservation[16,17]. Although brightness may decrease under cryogenic conditions, photobleaching rates are also reduced; this leads to prolonged observation times, which may be beneficial for some CLEM applications, as discussed below.

Data acquisition and overlay

Sequential acquisition and matching regions of interest (ROIs). Sample transfer between microscopes offers a free choice in FM modalities before EM, including wide-field, confocal and super-resolution FM. Because EM sample preparation can be performed after FM acquisition, there are many options for labeling and staining techniques that allow ultrastructural preservation and EM contrast, as they are not constrained by the need to preserve fluorescence. For cryogenic studies, dedicated sample holders for cooling have been developed for light microscopes that can then be transferred to a cryo-electron microscope[18–20]. Commercial versions are available at FEI (CryoStage[2]), Linkam (CMS196)[21] and Leica (Cryo CLEM)[17]. Matching the observed areas between modalities, or image registration, is essential for CLEM, and retrieval of an ROI identified with FM in the EM image has long been a major issue in correlative microscopy. Finder grids enable coarse alignment of a sample from live-cell observation to EM[22]. Commercial sample holders with navigation markers recognized by microscope software for automated ROI retrieval from Carl Zeiss (Shuttle & Find and Atlas5) and Jeol/Nikon (MiXcroscopy) are now available. The ROI can also be retrieved on the basis of LM data by means of virtual overlay[23], and both FEI (MAPS and CorrSight) and Jeol (JEM-1400Plus) provide recognition software. Three-dimensional (3D) alignment markers can be created in the sample by branding optical marks using laser irradiation, which are suitable for 3D CLEM[24]. Although these techniques do help to match areas, the accuracy they offer is too low for several applications.

High-precision overlay. For image overlay with accuracy better than 0.5 µm, fiducial markers identifiable in both LM and EM are needed. Several types of particles have been used for this purpose, including nanoparticles[25,26], quantum dots (QDs)[27] and polymer beads[7]. The use of multiple different fiducials may help cover different scales or account for chromatic distortions in multicolor microscopy[28]. Fiducials may be an integrated part of the sample (**Fig. 2a–c**) but are often only added for image registration. To preserve sample integrity, researchers can embed fiducials in a thin top layer below the sample[29] or create them with electron beam patterning[30]. However, in all these approaches, the overlay precision is limited by distortions introduced in the intermediate EM preparation steps.

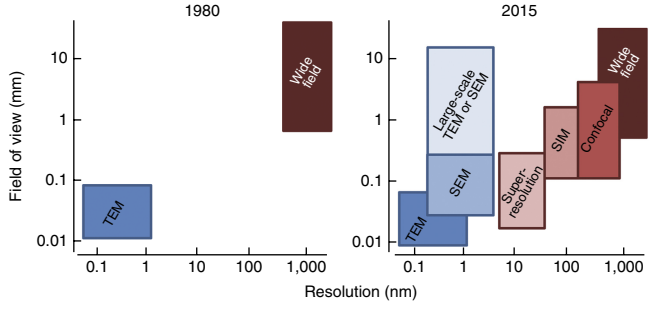


Figure 1 | Matching scales. The gap between EM (blue) and FM (red) in lateral dimensions has been filled by increasing the EM field of view, imaged at high resolution, mainly by automation and digitization, and by 'breaking' the FM diffraction limit, resulting in nearly matching scales for CLEM. Note that all FM and EM approaches depicted here can be used for CLEM. SIM, structured illumination microscopy.

© 2015 Nature America, Inc. All rights reserved.

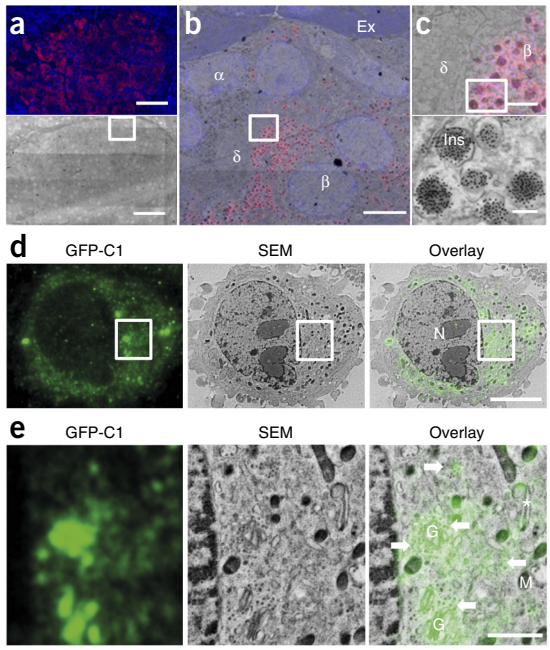


Figure 2 | Examples of CLEM with distinct approaches. (**a**–**c**) Post-embedding insulin immunolabeling (biotin-labeled antibodies) by QDs (streptavidin-conjugated QD655, red) and Hoechst counterstain (blue) of rat pancreas[74]. FM (top) followed by scanning EM (bottom) and overlay (**b**). (**c**) Boxed area from **b** (top) and magnification (bottom). Note the detection of the electron-dense nanoparticles. Ex, exocrine pancreas; α, alpha cell; β, beta cell; δ, delta cell; Ins, insulin granule. (**d**,**e**) Integrated microscopy (SECOM) of resin-embedded HeLa cells expressing GFP-C1, a diacylglycerol sensor, prepared with high-pressure freezing followed by freeze substitution[10]. Fluorescence from a 200-nm section (left), the matching back-scattered electron image (center) and the overlay (right) are shown. Note how precise subcellular localization of the fluorescent signal allows identification of corresponding structural features. (**e**) Detail from **d**, showing fluorescence corresponding to putative vesicular structures (arrows), Golgi networks and other highly curved membranous structures within the cytoplasm (asterisk). G, Golgi network; M, mitochondrion; N, nucleus. Images in **a**–**c** are our unpublished results; images in **d**,**e** are unpublished data kindly provided by C.J. Peddie and L.M. Collinson (Cancer Research UK). Scale bars: 50 µm (**a**), 5 µm (**b**,**d**), 1 µm and (**c**, top, and **e**) and 200 nm (**c**, bottom).

Integrated microscopy. Following initial development in the 1980s[31], commercial systems for integrated microscopy have appeared recently (**Fig. 4**). Integrated microscopes circumvent issues with ROI retrieval and registration markers, allowing inspection for rare events by LM and then EM analysis directly after. Because samples are not transferred between FM and EM acquisition, they should be both fluorescent and suitable for EM. As all preparation must therefore be done before inspection, sample distortion between FM and EM inspection is not an issue for the overlay image. FEI's iCorr, based on the iLEM prototype[32], is a single-color wide-field fluorescence microscope inside a transmission electron microscope (TEM). An objective lens with long working distance and low numerical aperture is placed between the pole pieces of the TEM lens. The fluorescence microscope serves to identify an ROI for TEM inspection on the basis of fluorescence. The sample is then rotated for TEM acquisition (**Fig. 4a**). The custom-made iLEM2 allows cryogenic examination of biosamples[16]. Delmic's SECOM is an inverted fluorescence microscope that can be retrofitted to a scanning electron microscope (SEM) such that the objective lens is below the sample, paraxial to the SEM (**Fig. 4b**). The SEM can then be used anywhere within the FM field of view (FOV)[10,15,31]. In the atmospheric SEM (ASEM, or Jeol's ClairScope)[33,34] and similar systems[35], the fluorescence microscope and SEM are also positioned in paraxial configuration, but with the SEM inverted. Only back-scattered electrons can be detected through a thin (50- to 100-nm) silicon nitride membrane[36,37], which seals the SEM vacuum chamber (**Fig. 4c**). The sample and the fluorescence microscope are both kept under atmospheric conditions, typically using water-dipping objectives. The lateral size of the membrane limits the observable area to several hundreds of micrometers[36,37]. Atmospheric inspection has been taken one step further in B-nano's airSEM, in which the sample is physically separated from the membrane vacuum seal[38,39] (**Fig. 4d**). As the sample is mounted on a translation stage, the observable area can be square centimeters. The fluorescence microscope or other systems, such as an atomic force microscope, can be positioned along the translation stage to allow correlative inspection with automated translation of an ROI between microscopes.

Depending on the goal and the microscope setup within reach, a proper choice of probe should be made, as addressed below.

PROBES FOR CLEM

Specific probes in microscopy typically consist of an affinity-based or genetically encoded targeting part, which identifies the protein of interest, linked to a label that is used for detection. CLEM has been pioneered by overlaying fluorescence images on top of the same region imaged by EM. All fluorescent markers available, including FPs, can be used to perform this kind of CLEM. This allows users to identify the underlying ultrastructure of the fluorescence label (**Figs. 2** and **5**). Higher-precision localization of the target proteins can be obtained by also visualizing the probe with EM through, for example, a sequential labeling step such as immunogold detection of GFP. Over the past two decades, probes, tags and other approaches have been developed to visualize molecules in both LM and EM (**Fig. 5**). These can be applied to the samples in either a pre-embedding or a post-embedding step.

A major advantage for immune-targeted affinity approaches is that they can be used to detect endogenous molecules in many contexts, including human tissue. However, fixation and permeabilization of cells to allow entrance of reagents is a prerequisite for these approaches, and these may cause obvious changes at the ultrastructural level[1]. Genetic tagging allows for non invasive labeling, thereby opening the door to a range of live-cell imaging applications[40,41], and is typically compatible with strong fixation to retain cellular systems intact, if fluorescence of the tag need not be retained[1]. Post-embedding immunolabeling of GFP with electron-dense particles, such as gold, can introduce EM contrast[13], but epitope availability upon EM preparation is often compromised[1]. Sequential LM and EM contrast can also be introduced in the form of osmiophilic diaminobenzidine (DAB) polymers, with polymerization induced by photo-oxidation, or enzymatically by peroxidases, as explained below. The benefit of CLEM is that fluorescence does not obscure any ultrastructural detail, whereas labeling with heavy metals (DAB, osmium

© 2015 Nature America, Inc. All rights reserved.

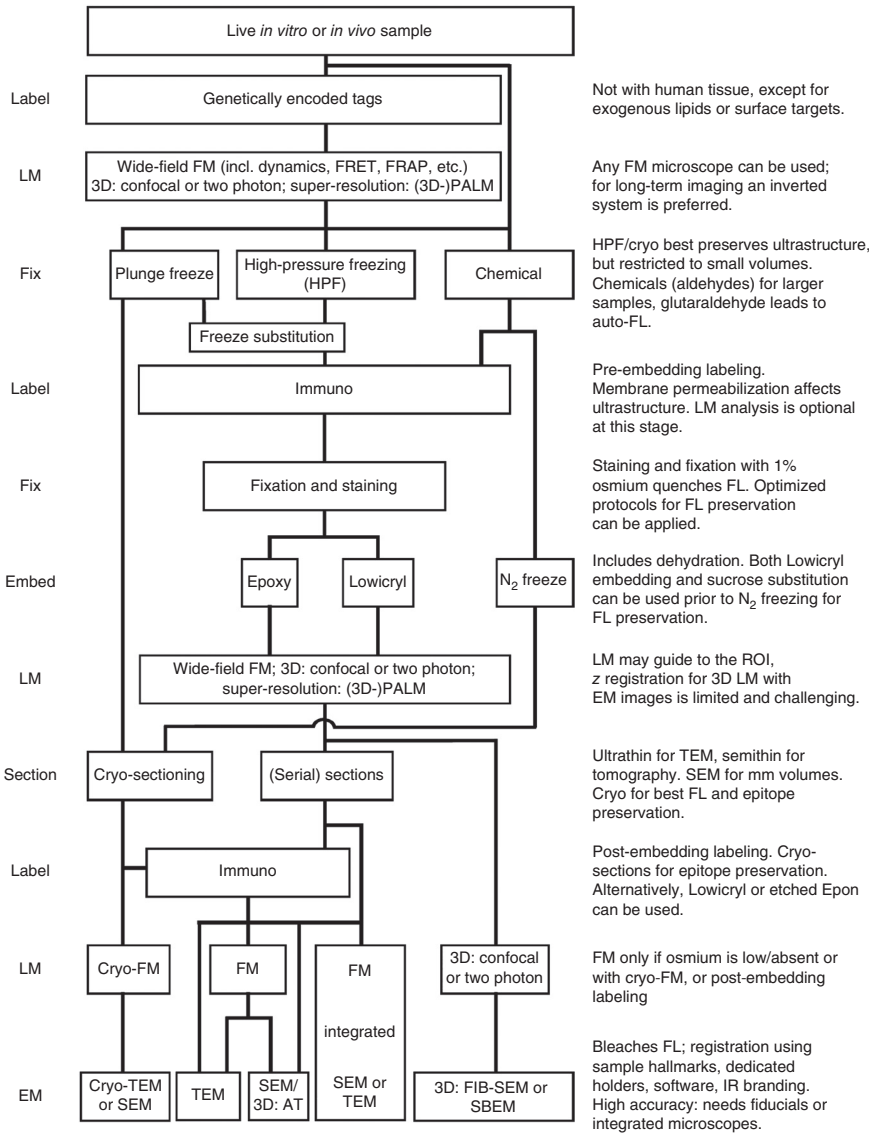


Figure 3 | CLEM procedures and considerations. A single flowchart for the numerous diverse CLEM applications cannot be given. The general layout is depicted (left), emphasizing considerations on the sample under study, preparation and preservation, as well as reagents and microscopes available (right). When choosing a certain trajectory (center), we recommend starting from previous achievements within the same field or from work that used the techniques of choice (**Supplementary Table 1**; references throughout the text). FRAP, fluorescence recovery after photobleaching; AT, array tomography; FL, fluorescence; IR, infrared.

or immunogold, or QDs) by definition will locally add label intensity to the original structural EM contrast (see, for example, the QDs in **Fig. 2c** versus fluorescence in **Fig. 2e**). We discuss the specific properties of the various probe types in more detail below.

Genetically encoded probes for pre-embedding labeling

Photo-oxidation. In the vicinity of a fluorophore, molecular dioxygen can be converted to singlet oxygen via excited-state energy transfer[42]. Upon addition of DAB, this singlet oxygen locally oxidizes the DAB, resulting in polymerization. Enhancement of DAB polymers with osmium creates an electron-dense label. Photo-oxidation has been pioneered using injected Lucifer yellow to label entire neurons[3]. Since then, molecules have been targeted using labeled lipids[43] or with antibodies[2].

The first genetically encoded system for CLEM using photo-oxidation was the tetracysteine tag, which could be incorporated into the protein of interest and then complexed with the biarsenical ReAsH; this approach has allowed for dynamic multicolor pulse-chase analysis, wherein a green dye is bound to all proteins of interest present. After washing and allowing time for new protein synthesis, the new, unlabeled, protein can then be identified by adding red dye. Because, in this case, only the red dye is photo-converted, the pulse-chase experiments allow for spatiotemporal analysis of the protein in EM[44] (**Fig. 5b**). However, improvement of other probes, including photoactivatable FPs that can also be used for pulse chase[45] (**Fig. 5d**), has limited the broad implementation of tetracysteine tagging, which is now used mainly when a small tag is needed to avoid interference with protein function. Also, synthetic fluorophores bound to genetically encoded tags (such as HaloTag and Snap-tag) are used for pulse chase[46], sometimes even allowing fluorescence preservation after embedding[47]. Finally, the mini singlet oxygen generator (miniSOG) system has been engineered as an entirely genetically encoded photo-oxidation CLEM probe[48,49] (**Fig. 5c**). A limitation of photo-oxidation is the requirement for light irradiation, which limits the volumes that can be analyzed and may be problematic for imaging thick tissues and organisms.

Peroxidases. Enzymatic DAB conversion by horseradish peroxidase (HRP) conjugated to antibodies has been widely used for labeling in EM[50]. However, implementation of genetically targeted HRP is limited to labeling proteins within the secretory route[51–53] because the active site of HRP does not form in the reducing environment of the mammalian cytosol. To bypass this limitation, researchers monomerized the cytosolic heme-dependent ascorbate peroxidase (APX), a plant homodimeric oxidase, and the active site was optimized for efficient DAB conversion, resulting in enhanced APX (APEX)[54] (**Fig. 5e**). APEX targeted to different cellular compartments, including the cytosol, nucleus and mitochondria, provides EM contrast[54]. However, expression levels of APEX that allow detectable DAB conversion have toxic side effects[55]. Improved APEX (APEX2) with higher DAB-conversion capability was developed[55] that can be used in lower concentrations to visualize targets, thus preventing cellular toxicity. APEX has also been combined with GFP tagging of connexin43 (ref. 54; **Fig. 5e**), providing a powerful probe for CLEM. APEX2 and miniSOG may also be targeted to proteins of interest using fluorescently labeled single-chain antibodies—as pioneered with 'fluobodies'[56], which are fusions of single-chain

© 2015 Nature America, Inc. All rights reserved.

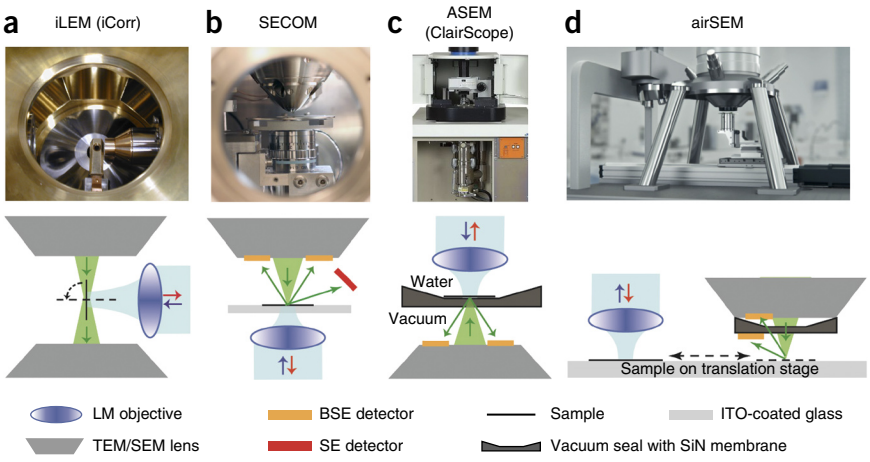


Figure 4 | Commercial integrated CLEM microscopes. The integrated systems (top) and schematic configuration (bottom) are shown. (**a**) The iLEM, commercialized as the iCorr, comprises an integrated FM microscope in a TEM. Optical imaging is followed by sample rotation for TEM acquisition. (**b**) SECOM has an integrated FM microscope in an SEM and inverted FM objective underneath the sample holder paraxial to the SEM column. (**c**) ASEM, commercialized as the ClairScope, has an FM microscope and SEM in paraxial configuration, with the FM microscope and sample under atmospheric conditions, sample cultured on a silicon nitride membrane with inverted SEM column underneath. (**d**) With airSEM, the sample is mounted on a translation stage for FM and scanning EM separated from the silicon nitride membrane; therefore, the electron beam travels a short distance through air. SE, secondary electrons; BSE, back-scattered electrons; ITO, indium tin oxide. Photographs reproduced from ref. 32, Elsevier (**a**); ref. 31, Wiley and the Royal Microscopical Society (**b**); Jeol Ltd. (**c**); and B-nano Ltd. (**d**).

© 2015 Nature America, Inc. All rights reserved.

variable fragments and GFP—although the use of fluobody-like approaches for CLEM remains to be demonstrated[57].

Metal tagging. Metallothionein and ferritin can be used as genetically encoded EM probes that bind to exogenously added metal atoms to form electron-dense clusters[58,59]. Implementation of these probes is uncommon because cells are grown under toxic, metal-rich conditions. Although metal tagging is usually applied in bacteria, which are more tolerant to heavy metals[59,60], this technique recently succeeded in mammalian cells for which a reduced metal-incubation time was used to prevent cellular toxicity[61].

Non–genetically encoded probes for pre-embedding labeling

Particles that are identifiable in EM but that are not genetically encoded, such as gold nanoparticles and QDs, can also be delivered to living cells. These may be taken up by cells: for example, by phagocytosis of nanoparticles or by endocytosis of ligand-bound particles. Alternatively, cells may first be more mildly fixed and permeabilized to immunolabel proteins inside[50], which can be beneficial for retaining epitopes or labeling in a 3D volume. However, good preservation of ultrastructure—a major benefit of pre-embedding labeling—is lost without strong fixation or when samples are permeabilized. Mild fixation and permeabilization can also lead to protein extraction or relocalization[1]. Typically, immunolabeling is performed after embedding of samples.

Post-embedding labeling for fluorescence in EM sections

With post-embedding labeling, fluorescence can be added directly on the EM-embedded sections via immunolabeling (**Fig. 3**), but the antigenicity of target proteins can be compromised as a consequence of fixation with glutaraldehyde and resin infiltration. Post-embedding immunolabeling on EM sections can also be performed using the cryo-based Tokuyasu method optimized for CLEM[13]. With the Tokuyasu method, samples are fixed with aldehydes, dehydrated using sucrose as a cryoprotectant and frozen in liquid nitrogen in order to allow ultrathin cryo-sectioning. Subsequently, sections are thawed for immunolabeling. Of all the immunolabeling approaches, generally the Tokuyasu method is used because it yields good morphology and epitope presentation and is relatively easy to use. An advantage of using ultrathin (~60-nm) sections is that fluorescence is emitted with better z resolution than those attainable with optical techniques such as confocal microscopy[23,62].

As a more advanced but also more time-consuming technique (sample preparation takes >1 week), high-pressure freezing (HPF) followed by freeze substitution (FS) and either plastic embedding or the Tokuyasu procedure may also be applied. This typically provides better preservation of ultrastructure and epitopes[63] than traditional chemical fixation, including Tokuyasu alone and epoxy embedding. In the case when pre-embedding FPs have been used, HPF-FS best preserves fluorescence. Sections may then be immunolabeled with FluoroNanogold and QDs, which are well-suited for combinatorial CLEM (**Fig. 5f**), although FluoroNanogold may require silver enhancement to increase EM contrast after FM acquisition[23,50]. The size-dependent emission spectra of QDs allow up to three targets to be distinguished at both the LM and EM levels[4]. The number of identifiable targets may be increased using shape-diverse nanoparticle probes[64] or by combining different probes. QDs can also be used for analysis of metal replicas when studying cell surface molecules or structures underneath the plasma membrane after either extraction by detergents or use of an ultrasonic burst—so-called unroofing of cells—to expose the adherent membrane[26,65].

SUPER-RESOLUTION FLUORESCENCE CLEM

A major limitation of localization of molecules by LM is the diffraction limit of light, which precludes localization at the biomolecular (i.e., nanometer) scale. A number of super-resolution techniques have been developed that allow localization with resolution below 50 nm, approaching EM scales[66,67]. Super-resolution techniques either (i) exploit shaped illumination beams that control depletion or saturation of molecular fluorescence energy levels or (ii) use stochastic or photoactivated switching of fluorophores in wide-field FM followed by post-acquisition localization. However, as with diffraction-limited microscopy, only labeled proteins or structures are visible in super-resolution FM, leaving the necessary cellular context in the dark. The first approaches to study this cellular context used sequential super-resolved FM and EM[68] (**Fig. 6**). FP photoactivation–based

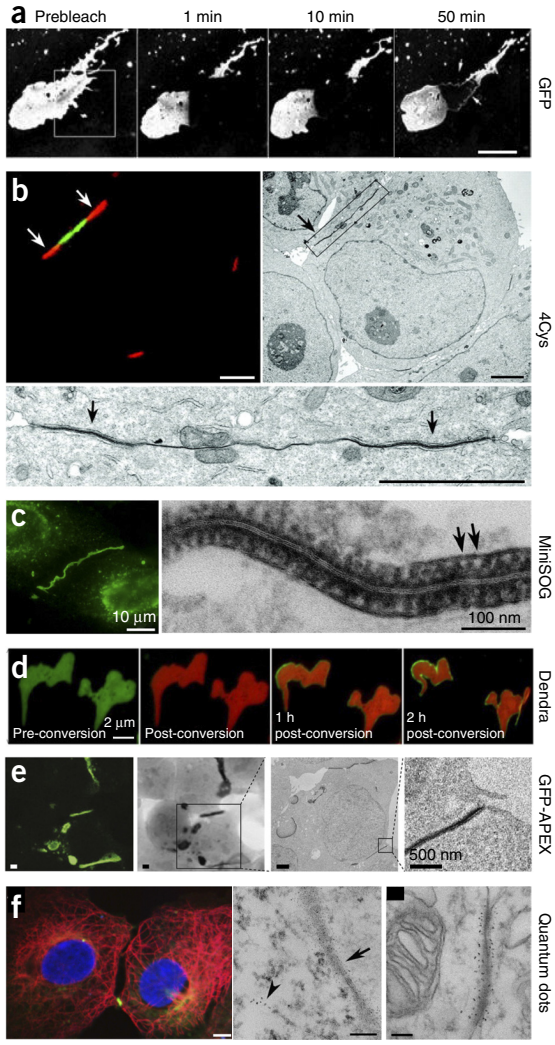


Figure 5 | Cx43 as a 'guinea pig' in CLEM probe development. Cx43 (connexin 43) forms gap junctions that allow diffusion of small molecules between cells. (**a**) Fluorescence recovery after photobleaching of GFP-tagged Cx43 revealed that gap junctions are reconstituted from the periphery. (**b**) Top left: tetracysteine-tagged Cx43 was labeled with FlAsH (green) for 4 h, and then newly synthesized protein was labeled with ReAsH (red) to reveal the same result. In this case, the older protein is not photobleached, and photoconversion of ReAsH allows for imaging with CLEM (top right). A concentrated precipitate of osmiophilic DAB polymers is present only at the edge of the gap junction (bottom), indicated with arrows. Note that four point mutations allow tetracysteine-labeling of Cx43 (ref. 111). (**c**) MiniSOG-tagged Cx43 allows for fluorescence inspection (left) followed by photoconversion and EM examination (right). Arrows indicate single connexons. (**d**) Pulse-chase analysis with photoactivatable FPs. Following expression (far left), conversion (center left) and chase for 1 h (center right) to 2 h (far right), gap junction plaque growth is detected at the periphery. With functional photoactivatable FPs in EM sections, the newly synthesized protein could be localized with high precision. (**e**) Imaging of Cx43 with APEX. APEX does not need an affinity step, nor photoconversion, for Cx43 analysis using EM. For LM analysis, a GFP tag was used in tandem, making the complete tag larger than Cx43. (**f**) Endogenous Cx43 (green; arrow) visualized with QDs and counterstained with QDs for microtubules (red; arrowhead) and Hoechst (blue). In cell culture the ultrastructure is affected by permeabilization and milder fixation compared to in the genetic approaches in **a**–**e**. However, tissue analysis with immunolabeling is most generic and most straightforward (right, mouse cerebellum). Scale bars: 3 µm (**a**), 0.5 µm (**b**), 1 µm (**f**, FM), 0.1 µm (**f**, EM). Images reproduced from ref. 112, copyright (2002) National Academy of Sciences, USA (**a**); ref. 44, AAAS (**b**); ref. 48 (**c**); ref. 45 (**d**); ref. 54, Nature Publishing Group (**e**); ref. 113, Springer (**f**, left and center); and ref. 4, Nature Publishing Group (**f**, right).

super-resolution CLEM on thin sections requires preservation of FP fluorescence during sample preparation for EM. Several approaches to achieve preservation have been reported. The first is to reduce the osmium tetroxide (OsO_4) concentration to a level that prevents fluorescence quenching but still provides sufficient membrane fixation and contrast, and to also optimize the embedding resin for fluorescence preservation[8]. This approach was used with both PALM (photoactivated localization microscopy)[68] and STED (stimulated emission depletion)[8,9]. Imaging was later improved using HPF and further uranylacetate staining after PALM to improve SEM contrast[9]. The second approach is to perform PALM, or STORM (stochastic optical reconstruction microscopy)[70], after Tokuyasu sectioning and to increase EM contrast of the sections after PALM with OsO_4 (refs. 25,29). Most recently, preservation of the fluorescence and photoswitching properties of the FP mEos4 was achieved after 0.5–1% OsO_4 treatment and resin embedding[11]. Cryofixation prevents fluorescence quenching and has been exploited for super-resolution CLEM. To avoid laser-induced heating during fluorescence imaging and subsequent ice crystallization within the sample, researchers have used cryoprotectants and pulsed laser illumination to allow heat dissipation[71]. Another concern for cryo-PALM is the reduced photoactivation and photobleaching rates under cryogenic temperature (80 K) conditions. So far, only photoactivatable GFP has been seen to retain its photoswitching capability under cryogenic conditions[71], and unless new photoactivatable FPs are developed, multicolor cryo-PALM is beyond reach.

MATCHING SCALES AND VOLUMES

Whereas super-resolution FM is moving LM resolution toward that of EM, progress in large-scale and 3D EM[72] has further bridged the two microscopy modalities (**Fig. 1**). EM data are typically represented as snapshots of cells or structures of interest with high resolution. This intrinsically restricts the FOV of the resulting image, which can, however, be overcome by manually stitching these snapshots together. Only recently, specific protocols have been developed to allow 2D automated TEM acquisition and stitching of areas up to 1 mm^2 at macromolecular resolution[52,73,74], an approach also referred to as nanotomy (for nano-anatomy; http://www.nanotomy.org/). With scanning-based detection (scanning EM), even larger FOVs (for example, 32,000 × 32,000 pixels) can be acquired with quality similar to that of transmission EM[75,76]. Analysis of these large data sets remains a bottleneck; this is still typically done by manual annotation, sometimes by many people[77]. In the future, automated data analysis will be guided by, and benefit from, applying CLEM to identify cellular or subcellular details or molecules.

Improvements in throughput of EM in the *z* direction are also critical for development of 3D CLEM. Volume reconstructions with EM[78] can be achieved with array tomography using serial sections[62] but also with serial block-face scanning EM (SBEM)[79] or focused-ion-beam scanning EM (FIB-SEM)[78]. With the latter two techniques, the upper surface of the sample is imaged and is then removed using an integrated ultramicrotome (SBEM) or an ion beam (FIB-SEM); this is followed by another imaging step,

© 2015 Nature America, Inc. All rights reserved.

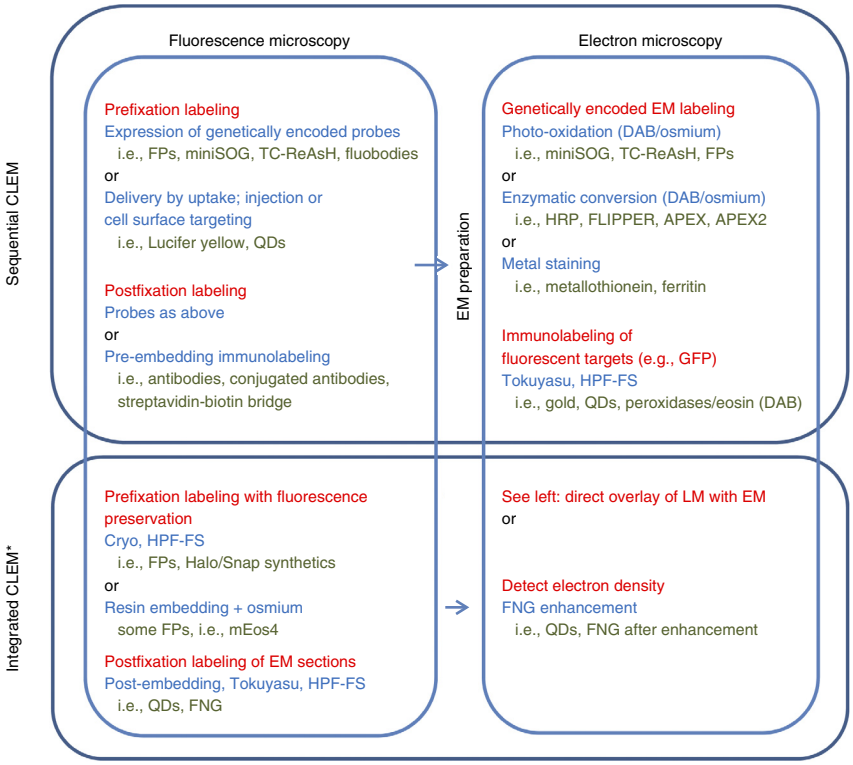


Figure 6 | Sequential versus integrated CLEM. Labeling and preparation approaches compatible with sequential (top) or integrated (bottom) CLEM inspection are compared. FM (left) is generally performed before EM (right). The opportunities have been grouped according to approaches (red); where sample preparation or labeling method (blue) and the choice of the right probes (green) is crucial to reach one's goal. *All samples for integrated microscopy can be used for sequential CLEM. FNG, FluoroNanogold.

and the process is repeated until the entire sample is imaged. A similar procedure has recently been used in LM to allow *ex vivo* FM of a whole mouse brain[80] by combining block-face imaging using two-photon excitation and subsequent removal of the acquired area with an ultramicrotome to access the next section. FIB-SEM has also been used to sculpt thin lamellae out of a 3D block for electron tomography[81]. Both SBEM and FIB-SEM can potentially be combined with CLEM.

Although a comprehensive review of 3D methods is out of the scope of this manuscript, common 3D CLEM approaches are (i) pre-embedding FM before EM processing and 3D analysis using either serial sections or block-face methods[82–84]; (ii) post-embedding labeling of serial sections[23,62]; and (iii) preservation of fluorescence upon EM preparation, either for serial sections (**Fig. 2d**,**e**) or for *en bloc* confocal microscopy followed by SBEM or FIB-SEM[21,23,85] (**Fig. 3**). With both pre-embedding and *en bloc* FM, fluorescence resolution along the *z* axis is limited (~1 µm). When serial ultrathin (40- to 100-nm) sections are labeled[62], this is improved to the section thickness. For samples prepared cryogenically to preserve FP fluorescence[6,7,10,12,16], integrated serial 3D CLEM using EM sections allows simultaneous matching of multiple FM and EM scales (**Fig. 2d**,**e**) both toward higher FM resolution and larger EM volumes, thus narrowing the volume gap in CLEM (**Fig. 1**). This enables diffraction-limited analysis of volumes of ~1 cm^3 by LM[80,86] and several cubic millimeters by EM. Note that scanning these volumes will take typically several hours to weeks, mainly depending on the voxel size and volume imaged.

GUIDELINES, TIPS AND TRICKS

Choosing a suitable CLEM approach clearly depends on the problem that needs to be tackled and the samples (cells, animals or biomaterial) being examined. We discuss here the most feasible approaches depending on the type of biological sample and give examples in which CLEM has been successfully used (**Fig. 6** and **Supplementary Table 1**). As the gap junction protein Cx43 has been extensively used to optimize and validate new probes, results from different approaches on this protein are shown (**Fig. 5**).

Human tissue

The most versatile method to target endogenous proteins within human tissue is immunolabeling. The major question is whether to perform the labeling pre-embedding or post-embedding or to use a combination of methods. Pre-embedding labeling with an antibody with a small fluorophore permits 3D or large-area FM and may also be used for super-resolution FM. In pre-embedding labeling, label penetration is an issue and will typically require permeabilization, relatively mild fixation (no or low glutaraldehyde) and prolonged incubation to get reagents inside[1]. The penetration efficiency depends on which tissue is probed, which permeabilization reagents are used and the size of probes. Whereas antibodies conjugated to small fluorophores or to HRP will typically penetrate tens of micrometers, larger particles such as QDs will be limited to several micrometers, and immunogold will not penetrate at all[4].

Post-embedding labeling may be a better option when the ROI does not require prior FM-based examination and selection or when colloidal gold is being used. The limiting step here is typically antigen recognition by the antibodies. Cryo-EM and Tokuyasu labeling is still the gold standard for identifying targets[13]. In addition, plastic-embedded material may be etched and subsequently used for immunolabeling (**Fig. 2**). The major decision will depend on what approach preserves epitope recognition, which typically needs to be addressed empirically—for example, by testing multiple antibodies against the same target, as they may react completely differently. As for pre-embedding labeling, the use of non-optimal concentrations of glutaraldehyde to preserve ultrastructure may help to retain antigenicity. Detection can then be achieved using labels visible by both FM and EM, such as QDs or FluoroNanogold. If LM is needed for a study but a fluorescence signal is not additive, consider using conventional histochemistry or nonfluorescent labels that are readily identifiable with LM, such as detection of colloidal gold using reflection microscopy or deposition of osmiophilic DAB polymers using HRP-conjugated antibodies. In select cases research is performed on *ex vivo* living human material, which allows for genetically

© 2015 Nature America, Inc. All rights reserved.

encoded tag delivery using transfection or transduction or by mechanical means (such as microinjection of material or gene gun–based delivery)[87].

Nonhuman tissue

In principle, all approaches discussed for human tissue can be used—and one is usually limited to these approaches—when studying endogenous proteins in nonhuman samples as well. A major benefit of using tissue samples from organisms that can be genetically modified, however, is the ability to use genetically encoded tags (**Supplementary Table 1c**). For CLEM of genetically modified organisms, overlaying the FP signal with EM, or the Tokuyasu-FP combination discussed above, is most commonly used.

Mammalian cell culture

Mammalian cells under *in vitro* culture conditions are well suited for immunobased approaches, especially to detect endogenous proteins. Alternatively, genetically encoded probes can be introduced. Genetically encoded CLEM probes, such as tetracysteines[88] or APEX2 (ref. 55), HRP[53] or miniSOG[48] fused to FPs, are suitable for live-cell imaging followed by EM analysis; ultrastructural preservation is uncompromised owing to the use of high glutaraldehyde and osmium concentrations[44,48,53,55,88]. Mammalian cells are also used in super-resolution FM followed by overlay with EM, for example with PALM[68], including the use of the optimized photoswitchable Eos4 protein[11]. With optimized protocols for fluorescence retention in thin sections, including the aforementioned cryotechniques[6,7,10,12], sample preparation resulting in deformation is no longer needed. This makes image registration less troublesome, and the samples may be used in integrated systems.

Microorganisms and viruses

For microorganisms such as yeast, bacteria and viruses, high resolution, but not tissue context, is typically needed, precluding the need for large FOVs. Imaging such microorganisms may be achieved by all CLEM approaches discussed above. In addition, bacteria have been used to pioneer toxic regiments such as metal tagging[59,60]. The small size of microorganisms makes them well suited for cryo-EM[59]. In some cases, the size of introduced genetically encoded tags may raise issues, in addition to problems that may arise from protein fusion and overexpression. For small, compact units, such as viruses, the use of peptide tags[89] may be preferred over protein tags to allow a normal life cycle.

Hardware

On the basis of the sample-preparation approach, one may be bound to sequential acquisition or instead have a choice between sequential or integrated CLEM (**Figs. 3** and **6**). When tissue samples are evaluated with sequential acquisition, it may not be necessary to turn to fiducials or finder grids if submicrometer overlay accuracy is not needed. Instead, during LM, pay attention to structures such as blood vessels or nuclei to help relocate the ROI, or turn to automated commercial solutions (see above: Data acquisition and overlay). When fluorescence is used, we recommend a nuclear stain, such as Hoechst or 4′,6-diamidino-2-phenylindole (DAPI), which will help to locate the nuclei in FM, as these organelles are easily recognized in EM (**Fig. 2**). For cellular samples, it is advisable to use marked grids or any of the available commercial systems for ROI retrieval. If an integrated approach is feasible, this may speed up acquisition time and improve throughput, but it imposes restrictions on the available sample-preparation techniques that need to preserve fluorescence and restricts FM and EM modalities to those present in the integrated system. iCorr is the only system available for TEM inspection, whereas SECOM fits with a current trend toward SEM use in biological applications, notably in high-content EM. Sample translation systems (iCorr or airSEM) need fiducials for high-accuracy overlay; in paraxial systems (SECOM or ClairScope) these can be omitted. In the SEM systems, the fluorescence microscope can be relatively freely operated, which may make the need for an advanced stand-alone microscope redundant. Also, systems such as airSEM and SECOM can be used upstream of other approaches, allowing additional results to be obtained[39,69] (**Fig. 6**). The ClairScope seems most suitable for inspection of cells in culture medium, staying close to live-cell FM. Importantly, although it is feasible to image live cells with these systems, it should be noted that electron irradiation during EM is highly toxic and will kill the cells. Nevertheless, this and other possibilities offered by integrated microscopes may provide novel roads for CLEM development.

Opportunities, considerations and limitations

CLEM adds resolution and cellular context to LM observations and adds dynamics and target identification to EM observations. Super-resolution LM techniques need EM to provide context to either pointillist PALM images[8,11,25,29,68] or STED data[8]. As a result, experiments based on CLEM are beginning to provide insight in several biological contexts.

For instance, gap junction turnover using pulse-chase labeling combined with dynamic imaging revealed the growth of these channels from the outside of the plaque at the EM and LM level (**Fig. 5** and references therein). Also, surprising variation in nuclear pore symmetry has been uncovered by applying fluorescence for quantification in a CLEM approach[90]. Similarly, not only the birth of the Golgi apparatus[88] but also trafficking of Golgi intermediates as tubular-saccular structures[91] have been clarified using LM dynamics and EM resolution in CLEM. The approach is also being used to study biology at the tissue level, such as understanding the sub-diffraction-limited connections in neuronal networks[84].

As CLEM paves the way for adding dimensions to data sets, choices for CLEM (**Fig. 3**) should be made according to the kind and size of material, whether pre- or post-embedding labeling applies, epitope recognition, and/or availability of genetically encoded tags. Thus, implementation of CLEM is guided by several considerations—mainly based on the research question at stake and models available, as well as access to microscopes. The benefits and limitations in a CLEM workflow are highlighted in **Figure 3** and discussed in more detail in earlier paragraphs. As a starting point, we suggest implementation of CLEM techniques used by others in the same research field or using similar models (**Supplementary Table 1** and references therein).

FUTURE OUTLOOK

Probes and live-cell electron microscopy

In most genetically encoded approaches, the protein of interest is tagged and overexpressed, which may cause artifacts.

© 2015 Nature America, Inc. All rights reserved.

Efforts to minimize such artifacts are ongoing: detrimental effects of genetically encoded tags may be prevented by improving their photophysical properties, thus requiring fewer labeled molecules to visualize targets, as shown with APEX2 improvement over APEX in cells[55]. Recently, fluorescence preservation of the newly developed photoactivatable FP mEos4 was shown[11]. With new targeted gene-modification tools such as the CRISPR (clustered, regularly interspaced, short palindromic repeats)-Cas9 system[92], the introduction of genetically encoded tags on endogenous proteins is becoming increasingly feasible. Further developments in fluobodies and the metallothionein approach are also being explored[61].

Cryo-EM comes the closest to imaging samples in a state similar to that observed with live-cell FM; however, the time needed for vitrification reduces FM-EM temporal correlation. Systems for rapid freezing of small samples during live-cell observation are in development[93]. Alternatively, liquid EM, in which ultrastructural analysis on cells in their original state is performed, is also being developed. In this approach, cells are cultured in a microfluidic chamber containing silicon nitride membranes that allow the electron beam to pass. Gold-conjugated ligand-receptor interactions over the complete cell surface have been observed with liquid scanning transmission EM[94]. The ultimate future perspective with combined FM and scanning EM in liquid would be to correlate live-cell imaging directly with an ultrastructural snapshot, the recording of which will deliver a lethal dose to the system under study. Liquid CLEM can be conducted by quickly transferring the microfluidic chamber between microscopes[95], but instrumentation for integrated liquid CLEM, to match the EM snapshot with FM acquisitions in time, is also emerging[34].

Development of vital EM probes would benefit CLEM not only for 'wet' EM but also for intravital applications. For instance, multiphoton microscopy, which achieves relatively deep penetration, may be used for intravital imaging of animal models and correlated to a later acquired EM image[96,97]. Improvements of intravital FM—including fast, high-throughput 3D fluorescence imaging approaches such as light-sheet microscopy[86]—may be applied, and relocating ROIs using laser-based marks ('tattooing')[96] will be important for intravital CLEM. With EM, structural information within whole living organisms can be obtained, as has been applied to study zebrafish[98–100], mouse neuronal circuits[101] and tumor cell invasion in mice[97].

Hardware and software solutions

High-content EM imaging (large FOV, high resolution, 3D) is still limited by acquisition time. Although obtaining serial sections for 3D imaging has been facilitated by developments such as an automatic tape-collecting microtome[102], and although, with SBEM and FIB-SEM, serial sectioning may be bypassed, faster approaches for data collection are still needed and are ongoing. For instance, multibeam scanning EM[103,104] and multi-energy deconvolution scanning EM[103] lead to an increase of at least one order of magnitude in acquisition speeds. High-content machines typically run 24/7, thereby limiting the number of samples that can be analyzed. Although application of high-content 2D and 3D CLEM is increasing, software development for reconstruction and analysis is required. In order to obtain high-content CLEM data, where the extent of EM analysis matches the FM scale, researchers can apply large-scale 2D and 3D EM reconstruction approaches. For recognition of EM structures, semiautomated software is being developed, such as Ilastik[101] and TrakEM2 (ref. 105), but a routine automated solution is not available yet.

Closing the mesoscale gap

A recent development in 3D imaging is the application of soft X-ray microscopy to biological samples[106,107]; 40-nm^3-resolution images with a lateral FOV of 20 µm and 10-µm depth have been obtained using this approach. By correlating soft X-ray microscopy with FM, researchers could image endosomes and phagosomes in cryofixed cells with high resolution[108]. Further correlation with high-magnification EM will create another way to cross scales from large-volume whole-organism FM to ultrastructural EM detail. In addition, integrated microscopes allow for cathodoluminescence (CL) examination, with which EM beam excitation of a probe results in light emission[109]. The emitted light spot can be correlated to the position of the electron beam, providing optimal simultaneous CLEM and making it possible to define the underlying structure. Application of this method will require biofunctionalization of CL probes, which should be pioneered in fixed specimens. Nanoparticles with distinct CL emission spectra[109] and CL protocols[110] will aid in future application of CL-CLEM in the biosciences.

CONCLUDING REMARKS

Imaging molecules in time and 3D space has transformed LM into a powerful biological research tool. With the development of combinatorial probes, tags, approaches and microscopes—including integrated systems—for CLEM, these experiments can be further put in their ultrastructural context. In parallel, super-resolution fluorescence techniques have moved FM resolution, now up to 20 nm, toward that of EM, allowing for higher-resolution localization solely with fluorescent probes. Conversely, with the increasing use of automated transmission EM, scanning EM and automated tiling software, EM acquisition size can match scales with conventional LM in both the planar and *z* directions, providing high-content CLEM images. Given these ongoing developments, we foresee broad implementation and a bright future for CLEM.

Note: Any Supplementary Information and Source Data files are available in the online version of the paper.

ACKNOWLEDGMENTS

We thank C.J. Peddie and L.M. Collinson for providing **Figure 2d,e** and our departmental members for feedback. We acknowledge financial support for our CLEM work from the Netherlands Organization for Scientific Research (ZonMW91111006; "Microscopy Valley" STW12718 and STW12714; NWO175-010-2009-023), the NanoNextNL innovation programme (09A.04) and a Marie Curie International Reintegration Grant within the 7th European Community Framework Program.

COMPETING FINANCIAL INTERESTS

The authors declare competing financial interests: details are available in the online version of the paper.

Reprints and permissions information is available online at http://www.nature.com/reprints/index.html.

1. Schnell, U., Dijk, F., Sjollema, K.A. & Giepmans, B.N. Immunolabeling artifacts and the need for live-cell imaging. *Nat. Methods* **9**, 152–158 (2012).
2. Deerinck, T.J. *et al.* Fluorescence photooxidation with eosin: a method for high resolution immunolocalization and *in situ* hybridization detection for light and electron microscopy. *J. Cell Biol.* **126**, 901–910 (1994).

© 2015 Nature America, Inc. All rights reserved.

3. Maranto, A.R. Neuronal mapping: a photooxidation reaction makes Lucifer yellow useful for electron microscopy. *Science* **217**, 953–955 (1982).
4. Giepmans, B.N., Deerinck, T.J., Smarr, B.L., Jones, Y.Z. & Ellisman, M.H. Correlated light and electron microscopic imaging of multiple endogenous proteins using quantum dots. *Nat. Methods* **2**, 743–749 (2005).
5. Karreman, M.A. *et al.* Optimizing immuno-labeling for correlative fluorescence and electron microscopy on a single specimen. *J. Struct. Biol.* **180**, 382–386 (2012).
6. Kukulski, W. *et al.* Correlated fluorescence and 3D electron microscopy with high sensitivity and spatial precision. *J. Cell Biol.* **192**, 111–119 (2011).
7. Kukulski, W. *et al.* Precise, correlated fluorescence microscopy and electron tomography of Lowicryl sections using fluorescent fiducial markers. *Methods Cell Biol.* **111**, 235–257 (2012).
8. Watanabe, S. *et al.* Protein localization in electron micrographs using fluorescence nanoscopy. *Nat. Methods* **8**, 80–84 (2011).
9. Watanabe, S. *et al.* Nano-fEM: protein localization using photo-activated localization microscopy and electron microscopy. *J. Vis. Exp.* **70**, e3995 (2012).
10. Peddie, C.J. *et al.* Correlative and integrated light and electron microscopy of in-resin GFP fluorescence, used to localise diacylglycerol in mammalian cells. *Ultramicroscopy* **143**, 3–14 (2014).
11. Paez-Segala, M.G. *et al.* Fixation-resistant photoactivatable fluorescent proteins for CLEM. *Nat. Methods* **12**, 215–218 (2015).
12. Nixon, S.J. *et al.* A single method for cryofixation and correlative light, electron microscopy and tomography of zebrafish embryos. *Traffic* **10**, 131–136 (2009).
13. van Rijnsoever, C., Oorschot, V. & Klumperman, J. Correlative light-electron microscopy (CLEM) combining live-cell imaging and immunolabeling of ultrathin cryosections. *Nat. Methods* **5**, 973–980 (2008).
14. Karreman, M.A. *et al.* Discovery of a new RNA-containing nuclear structure in UVC-induced apoptotic cells by integrated laser electron microscopy. *Biol. Cell* **101**, 287–299 (2009).
15. Liv, N. *et al.* Simultaneous correlative scanning electron and high-NA fluorescence microscopy. *PLoS ONE* **8**, e55707 (2013).
16. Faas, F.G. *et al.* Localization of fluorescently labeled structures in frozen-hydrated samples using integrated light electron microscopy. *J. Struct. Biol.* **181**, 283–290 (2013).
17. Schorb, M. & Briggs, J.A. Correlated cryo-fluorescence and cryo-electron microscopy with high spatial precision and improved sensitivity. *Ultramicroscopy* **143**, 24–32 (2014).
18. van Driel, L.F., Valentijn, J.A., Valentijn, K.M., Koning, R.I. & Koster, A.J. Tools for correlative cryo-fluorescence microscopy and cryo-electron tomography applied to whole mitochondria in human endothelial cells. *Eur. J. Cell Biol.* **88**, 669–684 (2009).
19. Sartori, A. *et al.* Correlative microscopy: bridging the gap between fluorescence light microscopy and cryo-electron tomography. *J. Struct. Biol.* **160**, 135–145 (2007).
20. Schwartz, C.L., Sarbash, V.I., Ataullakhanov, F.I., McIntosh, J.R. & Nicastro, D. Cryo-fluorescence microscopy facilitates correlations between light and cryo-electron microscopy and reduces the rate of photobleaching. *J. Microsc.* **227**, 98–109 (2007).
21. Müller-Reichert, T. & Verkade, P. *Methods in Cell Biology* Vol. 124 (Elsevier, 2014).
22. Spiegelhalter, C., Laporte, J.F. & Schwab, Y. Correlative light and electron microscopy: from live cell dynamic to 3D ultrastructure. *Methods Mol. Biol.* **1117**, 485–501 (2014).
23. Müller-Reichert, T. & Verkade, P. *Methods in Cell Biology* Vol. 111 (Elsevier, 2012).
24. Bishop, D. *et al.* Near-infrared branding efficiently correlates light and electron microscopy. *Nat. Methods* **8**, 568–570 (2011).
25. Kopek, B.G., Shtengel, G., Xu, C.S., Clayton, D.A. & Hess, H.F. Correlative 3D superresolution fluorescence and electron microscopy reveal the relationship of mitochondrial nucleoids to membranes. *Proc. Natl. Acad. Sci. USA* **109**, 6136–6141 (2012).
26. Sochacki, K.A., Shtengel, G., van Engelenburg, S.B., Hess, H.F. & Taraska, J.W. Correlative super-resolution fluorescence and metal-replica transmission electron microscopy. *Nat. Methods* **11**, 305–308 (2014).
27. Masich, S., Ostberg, T., Norlen, L., Shupliakov, O. & Daneholt, B. A procedure to deposit fiducial markers on vitreous cryo-sections for cellular tomography. *J. Struct. Biol.* **156**, 461–468 (2006).
28. Schellenberger, P. *et al.* High-precision correlative fluorescence and electron cryo microscopy using two independent alignment markers. *Ultramicroscopy* **143**, 41–51 (2014).
29. Kopek, B.G., Shtengel, G., Grimm, J.B., Clayton, D.A. & Hess, H.F. Correlative photoactivated localization and scanning electron microscopy. *PLoS ONE* **8**, e77209 (2013).
30. Koning, R.I., Kutchoukov, V.G., Hagen, C.W. & Koster, A.J. Nanofabrication of a gold fiducial array on specimen support for electron tomography. *Ultramicroscopy* **135**, 99–104 (2013).
31. Zonnevylle, A.C. *et al.* Integration of a high-NA light microscope in a scanning electron microscope. *J. Microsc.* **252**, 58–70 (2013).
32. Agronskaia, A.V. *et al.* Integrated fluorescence and transmission electron microscopy. *J. Struct. Biol.* **164**, 183–189 (2008).
33. Nishiyama, H. *et al.* Atmospheric scanning electron microscope observes cells and tissues in open medium through silicon nitride film. *J. Struct. Biol.* **169**, 438–449 (2010).
34. Maruyama, Y., Ebihara, T., Nishiyama, H., Suga, M. & Sato, C. Immuno EM-OM correlative microscopy in solution by atmospheric scanning electron microscopy (ASEM). *J. Struct. Biol.* **180**, 259–270 (2012).
35. Nawa, Y. *et al.* Multi-color imaging of fluorescent nanodiamonds in living HeLa cells using direct electron-beam excitation. *ChemPhysChem* **15**, 721–726 (2014).
36. Ring, E.A., Peckys, D.B., Dukes, M.J., Baudoin, J.P. & de Jonge, N. Silicon nitride windows for electron microscopy of whole cells. *J. Microsc.* **243**, 273–283 (2011).
37. Nishiyama, H. *et al.* Atmospheric scanning electron microscope system with an open sample chamber: Configuration and applications. *Ultramicroscopy* **147**, 86–97 (2014).
38. Solomonov, I. *et al.* Introduction of correlative light and airSEM microscopy imaging for tissue research under ambient conditions. *Sci. Rep.* **4**, 5987 (2014).
39. Vidavsky, N. *et al.* Initial stages of calcium uptake and mineral deposition in sea urchin embryos. *Proc. Natl. Acad. Sci. USA* **111**, 39–44 (2014).
40. Giepmans, B.N., Adams, S.R., Ellisman, M.H. & Tsien, R.Y. The fluorescent toolbox for assessing protein location and function. *Science* **312**, 217–224 (2006).
41. Shaner, N.C., Patterson, G.H. & Davidson, M.W. Advances in fluorescent protein technology. *J. Cell Sci.* **120**, 4247–4260 (2007).
42. Ogilby, P.R. Singlet oxygen: there is indeed something new under the sun. *Chem. Soc. Rev.* **39**, 3181–3209 (2010).
43. Pagano, R.E., Sepanski, M.A. & Martin, O.C. Molecular trapping of a fluorescent ceramide analogue at the Golgi apparatus of fixed cells: interaction with endogenous lipids provides a trans-Golgi marker for both light and electron microscopy. *J. Cell Biol.* **109**, 2067–2079 (1989).
44. Gaietta, G. *et al.* Multicolor and electron microscopic imaging of connexin trafficking. *Science* **296**, 503–507 (2002).
45. Baker, S.M., Buckheit, R.W. III. & Falk, M.M. Green-to-red photoconvertible fluorescent proteins: tracking cell and protein dynamics on standard wide-field mercury arc-based microscopes. *BMC Cell Biol.* **11**, 15 (2010).
46. Jansen, L.E., Black, B.E., Foltz, D.R. & Cleveland, D.W. Propagation of centromeric chromatin requires exit from mitosis. *J. Cell Biol.* **176**, 795–805 (2007).
47. Perkovic, M. *et al.* Correlative light- and electron microscopy with chemical tags. *J. Struct. Biol.* **186**, 205–213 (2014).
48. Shu, X. *et al.* A genetically encoded tag for correlated light and electron microscopy of intact cells, tissues, and organisms. *PLoS Biol.* **9**, e1001041 (2011).
49. Boassa, D. *et al.* Mapping the subcellular distribution of α-synuclein in neurons using genetically encoded probes for correlated light and electron microscopy: implications for Parkinson's disease pathogenesis. *J. Neurosci.* **33**, 2605–2615 (2013).
50. Sosinsky, G.E., Giepmans, B.N., Deerinck, T.J., Gaietta, G.M. & Ellisman, M.H. Markers for correlated light and electron microscopy. *Methods Cell Biol.* **79**, 575–591 (2007).
51. Li, J., Wang, Y., Chiu, S.L. & Cline, H.T. Membrane targeted horseradish peroxidase as a marker for correlative fluorescence and electron microscopy studies. *Front. Neural Circuits* **4**, 6 (2010).
52. Atasoy, D. *et al.* A genetically specified connectomics approach applied to long-range feeding regulatory circuits. *Nat. Neurosci.* **17**, 1830–1839 (2014).
53. Kuipers, J. *et al.* FLIPPER, a combinatorial probe for quantitative correlated live imaging and electron microscopy. *Cell Tissue Res.* **360**, 61–70 (2015).
54. Martell, J.D. *et al.* Engineered ascorbate peroxidase as a genetically encoded reporter for electron microscopy. *Nat. Biotechnol.* **30**, 1143–1148 (2012).
55. Lam, S.S. *et al.* Directed evolution of APEX2 for electron microscopy and proximity labeling. *Nat. Methods* **12**, 51–54 (2015).

© 2015 Nature America, Inc. All rights reserved.

56. Rothbauer, U. *et al.* Targeting and tracing antigens in live cells with fluorescent nanobodies. *Nat. Methods* **3**, 887–889 (2006).
57. Mironova, K.E. *et al.* Genetically encoded immunophotosensitizer 4D5scFv-miniSOG is a highly selective agent for targeted photokilling of tumor cells *in vitro*. *Theranostics* **3**, 831–840 (2013).
58. Mercogliano, C.P. & DeRosier, D.J. Concatenated metallothionein as a clonable gold label for electron microscopy. *J. Struct. Biol.* **160**, 70–82 (2007).
59. Wang, Q., Mercogliano, C.P. & Lowe, J. A ferritin-based label for cellular electron cryotomography. *Structure* **19**, 147–154 (2011).
60. Diestra, E., Fontana, J., Guichard, P., Marco, S. & Risco, C. Visualization of proteins in intact cells with a clonable tag for electron microscopy. *J. Struct. Biol.* **165**, 157–168 (2009).
61. Risco, C. *et al.* Specific, sensitive, high-resolution detection of protein molecules in eukaryotic cells using metal-tagging transmission electron microscopy. *Structure* **20**, 759–766 (2012).
62. Micheva, K.D. & Smith, S.J. Array tomography: a new tool for imaging the molecular architecture and ultrastructure of neural circuits. *Neuron* **55**, 25–36 (2007).
63. McDonald, K.L. Rapid embedding methods into epoxy and LR White resins for morphological and immunological analysis of cryofixed biological specimens. *Microsc. Microanal.* **20**, 152–163 (2014).
64. Philimonenko, V.V. *et al.* Simultaneous detection of multiple targets for ultrastructural immunocytochemistry. *Histochem. Cell Biol.* **141**, 229–239 (2014).
65. Collins, A., Warrington, A., Taylor, K.A. & Svitkina, T. Structural organization of the actin cytoskeleton at sites of clathrin-mediated endocytosis. *Curr. Biol.* **21**, 1167–1175 (2011).
66. Deschout, H. *et al.* Precisely and accurately localizing single emitters in fluorescence microscopy. *Nat. Methods* **11**, 253–266 (2014).
67. Schermelleh, L., Heintzmann, R. & Leonhardt, H. A guide to super-resolution fluorescence microscopy. *J. Cell Biol.* **190**, 165–175 (2010).
68. Betzig, E. *et al.* Imaging intracellular fluorescent proteins at near-molecular resolution. *Science* **313**, 1642–1645 (2006).
69. Voorneveld, P.W. *et al.* Loss of SMAD4 alters BMP signaling to promote colorectal cancer cell metastasis via activation of Rho and ROCK. *Gastroenterology* **147**, 196–208.e13 (2014).
70. Suleiman, H. *et al.* Nanoscale protein architecture of the kidney glomerular basement membrane. *eLife* **2**, e01149 (2013).
71. Chang, Y.W. *et al.* Correlated cryogenic photoactivated localization microscopy and cryo-electron tomography. *Nat. Methods* **11**, 737–739 (2014).
72. Patwardhan, A. *et al.* A 3D cellular context for the macromolecular world. *Nat. Struct. Mol. Biol.* **21**, 841–845 (2014).
73. Faas, F.G. *et al.* Virtual nanoscopy: generation of ultra-large high resolution electron microscopy maps. *J. Cell Biol.* **198**, 457–469 (2012).
74. Ravelli, R.B. *et al.* Destruction of tissue, cells and organelles in type 1 diabetic rats presented at macromolecular resolution. *Sci. Rep.* **3**, 1804 (2013).
75. Kuwajima, M., Mendenhall, J.M., Lindsey, L.F. & Harris, K.M. Automated transmission-mode scanning electron microscopy (tSEM) for large volume analysis at nanoscale resolution. *PLoS ONE* **8**, e59573 (2013).
76. Sokol, E. *et al.* Large-scale electron microscopy maps of patient skin and mucosa provide insight into pathogenesis of blistering diseases. *J. Invest. Dermatol.* doi:10.1038/jid.2015.109 (9 April 2015).
77. Briggman, K.L., Helmstaedter, M. & Denk, W. Wiring specificity in the direction-selectivity circuit of the retina. *Nature* **471**, 183–188 (2011).
78. Briggman, K.L. & Bock, D.D. Volume electron microscopy for neuronal circuit reconstruction. *Curr. Opin. Neurobiol.* **22**, 154–161 (2012).
79. Denk, W. & Horstmann, H. Serial block-face scanning electron microscopy to reconstruct three-dimensional tissue nanostructure. *PLoS Biol.* **2**, e329 (2004).
80. Ragan, T. *et al.* Serial two-photon tomography for automated *ex vivo* mouse brain imaging. *Nat. Methods* **9**, 255–258 (2012).
81. Rigort, A. *et al.* Focused ion beam micromachining of eukaryotic cells for cryoelectron tomography. *Proc. Natl. Acad. Sci. USA* **109**, 4449–4454 (2012).
82. Murphy, G.E. *et al.* Correlative 3D imaging of whole mammalian cells with light and electron microscopy. *J. Struct. Biol.* **176**, 268–278 (2011).
83. Maco, B., Holtmaat, A., Jorstad, A., Fua, P. & Knott, G.W. Correlative *in vivo* 2-photon imaging and focused ion beam scanning electron microscopy: 3D analysis of neuronal ultrastructure. *Methods Cell Biol.* **124**, 339–361 (2014).
84. Bock, D.D. *et al.* Network anatomy and *in vivo* physiology of visual cortical neurons. *Nature* **471**, 177–182 (2011).
85. Narayan, K. *et al.* Multi-resolution correlative focused ion beam scanning electron microscopy: applications to cell biology. *J. Struct. Biol.* **185**, 278–284 (2014).
86. Chen, B.C. *et al.* Lattice light-sheet microscopy: imaging molecules to embryos at high spatiotemporal resolution. *Science* **346**, 1257998 (2014).
87. Arsenault, J. & O'Brien, J.A. Optimized heterologous transfection of viable adult organotypic brain slices using an enhanced gene gun. *BMC Res. Notes* **6**, 544 (2013).
88. Gaietta, G.M. *et al.* Golgi twins in late mitosis revealed by genetically encoded tags for live cell imaging and correlated electron microscopy. *Proc. Natl. Acad. Sci. USA* **103**, 17777–17782 (2006).
89. Lanman, J. *et al.* Visualizing flock house virus infection in *Drosophila* cells with correlated fluorescence and electron microscopy. *J. Struct. Biol.* **161**, 439–446 (2008).
90. Löschberger, A., Franke, C., Krohne, G., van de Linde, S. & Sauer, M. Correlative super-resolution fluorescence and electron microscopy of the nuclear pore complex with molecular resolution. *J. Cell Sci.* **127**, 4351–4355 (2014).
91. Polishchuk, R.S. *et al.* Correlative light-electron microscopy reveals the tubular-saccular ultrastructure of carriers operating between Golgi apparatus and plasma membrane. *J. Cell Biol.* **148**, 45–58 (2000).
92. Mali, P., Esvelt, K.M. & Church, G.M. Cas9 as a versatile tool for engineering biology. *Nat. Methods* **10**, 957–963 (2013).
93. Koning, R.I. *et al.* MAVIS: an integrated system for live microscopy and vitrification. *Ultramicroscopy* **143**, 67–76 (2014).
94. Peckys, D.B. & de Jonge, N. Liquid scanning transmission electron microscopy: imaging protein complexes in their native environment in whole eukaryotic cells. *Microsc. Microanal.* **20**, 346–365 (2014).
95. Dukes, M.J., Peckys, D.B. & de Jonge, N. Correlative fluorescence microscopy and scanning transmission electron microscopy of quantum-dot-labeled proteins in whole cells in liquid. *ACS Nano* **4**, 4110–4116 (2010).
96. Ritsma, L., Vrisekoop, N. & van Rheenen, J. *In vivo* imaging and histochemistry are combined in the cryosection labelling and intravital microscopy technique. *Nat. Commun.* **4**, 2366 (2013).
97. Karreman, M.A. *et al.* Correlating intravital multi-photon microscopy to 3D electron microscopy of invading tumor cells using anatomical reference points. *PLoS ONE* **9**, e114448 (2014).
98. Armer, H.E. *et al.* Imaging transient blood vessel fusion events in zebrafish by correlative volume electron microscopy. *PLoS ONE* **4**, e7716 (2009).
99. van Ham, T.J. *et al.* Intravital correlated microscopy reveals differential macrophage and microglial dynamics during resolution of neuroinflammation. *Dis. Model. Mech.* **7**, 857–869 (2014).
100. Hosseini, R. *et al.* Correlative light and electron microscopy imaging of autophagy in a zebrafish infection model. *Autophagy* **10**, 1844–1857 (2014).
101. Maco, B. *et al.* Semiautomated correlative 3D electron microscopy of *in vivo*-imaged axons and dendrites. *Nat. Protoc.* **9**, 1354–1366 (2014).
102. Hayworth, K.J. *et al.* Imaging ATUM ultrathin section libraries with WaferMapper: a multi-scale approach to EM reconstruction of neural circuits. *Front. Neural Circuits* **8**, 68 (2014).
103. Marx, V. Brain mapping in high resolution. *Nature* **503**, 147–152 (2013).
104. Eberle, A.L. *et al.* High-resolution, high-throughput imaging with a multibeam scanning electron microscope. *J. Microsc.* doi:10.1111/jmi.12224 (27 January 2015).
105. Cardona, A. *et al.* TrakEM2 software for neural circuit reconstruction. *PLoS ONE* **7**, e38011 (2012).
106. Duke, E., Dent, K., Razi, M. & Collinson, L.M. Biological applications of cryo-soft X-ray tomography. *J. Microsc.* **255**, 65–70 (2014).
107. Smith, E.A. *et al.* Correlative cryogenic tomography of cells using light and soft X-rays. *Ultramicroscopy* **143**, 33–40 (2014).
108. Duke, E.M. *et al.* Imaging endosomes and autophagosomes in whole mammalian cells using correlative cryo-fluorescence and cryo-soft X-ray microscopy (cryo-CLXM). *Ultramicroscopy* **143**, 77–87 (2014).
109. Glenn, D.R. *et al.* Correlative light and electron microscopy using cathodoluminescence from nanoparticles with distinguishable colours. *Sci. Rep.* **2**, 865 (2012).
110. Narváez, A.C., Weppelman, I.G.C., Moerland, R.J., Hoogenboom, J.P. & Kruit, P. Confocal filtering in cathodoluminescence microscopy of nanostructures. *Appl. Phys. Lett.* **104**, 251121 (2014).
111. Giepmans, B.N. Bridging fluorescence microscopy and electron microscopy. *Histochem. Cell Biol.* **130**, 211–217 (2008).
112. Lauf, U. *et al.* Dynamic trafficking and delivery of connexons to the plasma membrane and accretion to gap junctions in living cells. *Proc. Natl. Acad. Sci. USA* **99**, 10446–10451 (2002).
113. Deerinck, T.J., Giepmans, B.N., Smarr, B.L., Martone, M.E. & Ellisman, M.H. Light and electron microscopic localization of multiple proteins using quantum dots. *Methods Mol. Biol.* **374**, 43–53 (2007).

© 2015 Nature America, Inc. All rights reserved.

Pascal de Boer, Jacob P. Hoogenboom & Ben N. G. Giepmans (2015) **Correlated light and electron microscopy: Ultrastructure lights up!** Nature Methods. Supplementary table 1.

Table 1. Overview of CLEM implementation –Selected studies on different biomaterials and in different research fields as a reference when implementing CLEM

Field & use	CLEM approach or specifics	Ref
A. Human tissue		
Identifying axillary sweat gland structures	En bloc CLSM, serial section TEM	[1]
Skin (also connections and protrusion in colon cancer cells)	Integrated microscopy – FM-SEM	[2]
Reconstruction of kidney glomerular basement membrane	STORM-SEM	[3]
B. Non-human tissue		
Visualizing different cell types in mouse cerebellum	Pre-embedding QD-labeling	[4]
Golgi intermediates trafficking	GFP – HRP immunolabeling	[5]
Architecture and ultrastructure of neural circuits (mouse)	Array tomography (IF)	[6]
Wheat in intestine and peroxidases in liver (rat)	Integrated FM-TEM	[7]
Anatomy and physiology of visual cortex neurons	Intravital - large-scale 2D/ 3D CLEM	[8]
Mitochondria in *C. elegans* and synaptic adhesion (mouse)	MiniSOG	[9]
Visualization of pre-synaptic proteins in brain (rat)	GFP photo-oxidation	[10]
Calcium uptake and deposition in embryos (sea urchin)	iM – AirSEM	[11]
Blood vessel fusion (zebrafish)	Intravital – FIB/SEM	[12]
Macrophages vs. microglia in neuro-inflammation (zebrafish)	Intravital	[13]
Tumor cell invasion (mouse)	Intravital 3D CLEM	[14]
C.1 Eukaryotic cells – Primary cells		
RNA-containing nuclear structure in early apoptosis	iM – FM-TEM Tokuyasu labeling	[15]
α-synuclein localization in neurons	Tetracysteine/MiniSOG	[16]
Neuron differentiation, networking, phagocytosis	iM – ASEM fluorescent beads	[17]
C.2 Eukaryotic cells – Cell-lines		
Dynamics and trafficking of gap junctions	Pulse-chase TC-ReAsH/FlAsH	[18]
In mitotic cells four Golgi's are present	TC-ReAsH	[19]
Mitochondrial transformation during apoptosis	Live-cell, TC-FlAsH, TMRE; (3D) TEM	[20]
Identification of detergent resistant membrane rafts	Pre-embedding IF, TEM	[21]
Actin structure and clathrin mediated endocytosis	IF, metal-replica EM	[22]
Ca^{2+} sensor in ER; Cytoskeleton in growth cones and synapses	iM – ASEM, FNG immunolabeling	[23]
Diacylglycerol and nuclear envelope/ER reorganization in mitosis	Pre-embedding FM, TEM	[24]
Adhesion by synaptic neurexin and neuroligin	Pre-embedding FM, TEM	[25]
Mitochondrial structure and membrane relationship	PALM, followed by FIB-SEM	[26]
Connexin43 imaging	APEX-GFP fusion tag	[27]
mAtg9 in autophagy regulation	Combinatorial FPs + immunogold	[28]
Von Willebrand Factor remodeling during exocytosis	GFP, IF, TEM, tomography	[29]
CCCP as trigger for mitophagy	Live-cell CLSM, followed by TEM	[30]
GLUT4 expression, localization and quantification in adipocytes	Combinatorial GFP + immunogold	[31]
Autophagosome formation	Combinatorial GFP + immunogold	[32]
Diacylglycerol in nuclear envelope, reticulum and Golgi	iM – FM-SEM with GFP	[33]
Identification of endosomes and autophagosomes	cryo-FM and cryo-soft X-ray	[34]
Variation nuclear pore symmetrie	STORM – SEM	[35]
3D position of epsin on clathrin-coated structures	PALM – metal-replica EM	[36]
C.3 Eukaryotic cells – Unicellular organisms		
Plasma membrane reshaping during endocytosis in yeast	FPs; 3D EM, with fluorescence	[37]
Type VI secretion system of *Myxococcus xanthus*	Correlated 3D-PALM cryo-EM	[38]
Detailed Golgi architecture in *Saccharomyces cerevisiae*	3D CLEM by serial Tokuyasu	[39]
Polarized actin for sorting axonal and dendritic proteins	Membranes: phalloidin and SEM	[40]
D.1 Micro-organisms and viruses		
Chemosensory machinery and cell division in *e. coli*	GFP-ferritin	[41]
D.2 Micro-organisms and viruses – In cells		
Virus infection of mammalian cells	Fluorescent HIV, live-cell; FIB-SEM	[42]
Rubella virus-induced cell structures	Metallothionein tagging	[43]
Dynamics of HIV-containing compartments in macrophages	Live-cell FM; TEM	[44]
Infection of human skeletal muscle cells by Influenza A	Pre-embedding IF; TEM	[45]
Yersinia pseudotuberculosis during host infiltration	Pre-embedding fluorescence; TEM	[46]
D.3 Micro-organisms and viruses – In organisms		
Mycobacterium marinum containing granulomas in zebrafish	Pre-embedding FM; TEM	[47]
Requirement of importin-α7 for Influenza A replication (mice)	GFP-virus. CLSM, ESEM, TEM	[48]
E. Method books for CLEM		
Methods in Cell Biology volume 111, 2012	Various techniques	[49]
Methods in Cell Biology volume 124, 2014	Various techniques	[50]
Methods in Molecular Biology volume 1117, 2014	Various techniques	[51]

References

1. Wilke, K. *et al*. A strategy for correlative microscopy of large skin samples: towards a holistic view of axillary skin complexity. *Exp. Dermatol.* **17**, 73-81 (2008).

2. Liv, N. *et al*. Simultaneous Correlative Scanning Electron and High-NA Fluorescence Microscopy. *PLoS One* **8**, e55707 (2013).

3. Suleiman, H. *et al*. Nanoscale protein architecture of the kidney glomerular basement membrane. *Elife (Cambridge)* **2**, e01149 (2013).

4. Giepmans, B. N., Deerinck, T. J., Smarr, B. L., Jones, Y. Z. & Ellisman, M. H. Correlated light and electron microscopic imaging of multiple endogenous proteins using Quantum dots. *Nat Methods* **2**, 743-9 (2005).

5. Polishchuk, R. S. *et al*. Correlative light-electron microscopy reveals the tubular-saccular ultrastructure of carriers operating between Golgi apparatus and plasma membrane. *J. Cell Biol.* **148**, 45-58 (2000).

6. Micheva, K. D. & Smith, S. J. Array tomography: a new tool for imaging the molecular architecture and ultrastructure of neural circuits. *Neuron* **55**, 25-36 (2007).

7. Agronskaia, A. V. *et al*. Integrated fluorescence and transmission electron microscopy. *J. Struct. Biol.* **164**, 183-189 (2008).

8. Bock, D. D. *et al*. Network anatomy and in vivo physiology of visual cortical neurons. *Nature* **471**, 177-182 (2011).

9. Shu, X. *et al*. A genetically encoded tag for correlated light and electron microscopy of intact cells, tissues, and organisms. *PLoS Biol.* **9**, e1001041 (2011).

10. Horstmann, H., Vasileva, M. & Kuner, T. Photooxidation-guided ultrastructural identification and analysis of cells in neuronal tissue labeled with green fluorescent protein. *PLoS One* **8**, e64764 (2013).

11. Vidavsky, N. *et al*. Initial stages of calcium uptake and mineral deposition in sea urchin embryos. *Proc. Natl. Acad. Sci. U. S. A.* **111**, 39-44 (2014).

12. Armer, H. E. *et al*. Imaging transient blood vessel fusion events in zebrafish by correlative volume electron microscopy. *PLoS One* **4**, e7716 (2009).

13. van Ham, T. J. *et al*. Intravital correlated microscopy reveals differential macrophage and microglial dynamics during resolution of neuroinflammation. *Dis. Model. Mech.* **7**, 857-869 (2014).

14. Karreman, M. A. *et al*. Correlating intravital multi-photon microscopy to 3D electron microscopy of invading tumor cells using anatomical reference points. *PLoS One* **9**, e114448 (2014).

15. Karreman, M. A. *et al*. Discovery of a new RNA-containing nuclear structure in UVC-induced apoptotic cells by integrated laser electron microscopy. *Biol. Cell.* **101**, 287-299 (2009).

16. Boassa, D. *et al*. Mapping the subcellular distribution of alpha-synuclein in neurons using genetically encoded probes for correlated light and electron microscopy: implications for Parkinson's disease pathogenesis. *J. Neurosci.* **33**, 2605-2615 (2013).

17. Hirano, K. *et al*. Electron microscopy of primary cell cultures in solution and correlative optical microscopy using ASEM. *Ultramicroscopy* **143**, 52-66 (2014).

18. Gaietta, G. *et al*. Multicolor and electron microscopic imaging of connexin trafficking. *Science* **296**, 503-507 (2002).

19. Gaietta, G. M. *et al*. Golgi twins in late mitosis revealed by genetically encoded tags for live cell imaging and correlated electron microscopy. *Proc Natl Acad Sci U S A* **103**, 17777-177782 (2006).

20. Sun, M. G. *et al*. Correlated three-dimensional light and electron microscopy reveals transformation of mitochondria during apoptosis. *Nat. Cell Biol.* **9**, 1057-1065 (2007).

21. Jahn, K. A. & Braet, F. Monitoring membrane rafts in colorectal cancer cells by means of correlative fluorescence electron microscopy (CFEM). *Micron* **39**, 1393-1397 (2008).

22. Collins, A., Warrington, A., Taylor, K. A. & Svitkina, T. Structural organization of the actin cytoskeleton at sites of clathrin-mediated endocytosis. *Curr. Biol.* **21**, 1167-1175 (2011).

23. Maruyama, Y., Ebihara, T., Nishiyama, H., Suga, M. & Sato, C. Immuno EM-OM correlative microscopy in solution by atmospheric scanning electron microscopy (ASEM). *J. Struct. Biol.* **180**, 259-270 (2012).

24. Domart, M. C. *et al*. Acute manipulation of diacylglycerol reveals roles in nuclear envelope assembly & endoplasmic reticulum morphology. *PLoS One* **7**, e51150 (2012).

25. Tanaka, H. *et al*. Higher-order architecture of cell adhesion mediated by polymorphic synaptic adhesion molecules neurexin and neuroligin. *Cell. Rep.* **2**, 101-110 (2012).

26. Kopek, B. G., Shtengel, G., Xu, C. S., Clayton, D. A. & Hess, H. F. Correlative 3D superresolution fluorescence and electron microscopy reveal the relationship of mitochondrial nucleoids to membranes. *Proc. Natl. Acad. Sci. U. S. A.* **109**, 6136-6141 (2012).

27. Martell, J. D. *et al*. Engineered ascorbate peroxidase as a genetically encoded reporter for electron microscopy. *Nat. Biotechnol.* **30**, 1143-1148 (2012).

28. Orsi, A. *et al*. Dynamic and transient interactions of Atg9 with autophagosomes, but not membrane integration, are required for autophagy. *Mol. Biol. Cell* **23**, 1860-1873 (2012).

29. Mourik, M. J. *et al*. von Willebrand factor remodeling during exocytosis from vascular endothelial cells. *J. Thromb. Haemost.* **11**, 2009-2019 (2013).

30. Padman, B. S., Bach, M., Lucarelli, G., Prescott, M. & Ramm, G. The protonophore CCCP interferes with lysosomal degradation of autophagic cargo in yeast and mammalian cells. *Autophagy* **9**, 1862-1875 (2013).

31. Hodgson, L., Tavare, J. & Verkade, P. Development of a quantitative Correlative Light Electron Microscopy technique to study GLUT4 trafficking. *Protoplasma* **251**, 403-416 (2014).

32. Uemura, T. *et al*. A cluster of thin tubular structures mediates transformation of the endoplasmic reticulum to autophagic isolation membrane. *Mol. Cell. Biol.* **34**, 1695-1706 (2014).

33. Peddie, C. J. *et al*. Correlative and integrated light and electron microscopy of in-resin GFP fluorescence, used to localise diacylglycerol in mammalian cells. *Ultramicroscopy* **143**, 3-14 (2014).

34. Duke, E. M. *et al*. Imaging endosomes and autophagosomes in whole mammalian cells using correlative cryo-fluorescence and cryo-soft X-ray microscopy (cryo-CLXM). *Ultramicroscopy* **143**, 77-87 (2014).

35. Loschberger, A., Franke, C., Krohne, G., van de Linde, S. & Sauer, M. Correlative super-resolution fluorescence and electron microscopy of the nuclear pore complex with molecular resolution. *J. Cell. Sci.* **127**, 4351-4355 (2014).

36. Sochacki, K. A., Shtengel, G., van Engelenburg, S. B., Hess, H. F. & Taraska, J. W. Correlative super-resolution fluorescence and metal-replica transmission electron microscopy. *Nat. Methods* **11**, 305-308 (2014).

37. Kukulski, W. *et al*. Precise, correlated fluorescence microscopy and electron tomography of lowicryl sections using fluorescent fiducial markers. *Methods Cell Biol.* **111**, 235-257 (2012).

38. Chang, Y. W. *et al*. Correlated cryogenic photoactivated localization microscopy and cryo-electron tomography. *Nat. Methods* **11**, 737-739 (2014).

39. Mari, M., Geerts, W. J. & Reggiori, F. Immuno- and correlative light microscopy-electron tomography methods for 3D protein localization in yeast. *Traffic* **10**, 1164-1178 (2014).

40. Watanabe, K. *et al*. Networks of polarized actin filaments in the axon initial segment provide a mechanism for sorting axonal and dendritic proteins. *Cell. Rep.* **2**, 1546-1553 (2012).

41. Wang, Q., Mercogliano, C. P. & Lowe, J. A ferritin-based label for cellular electron cryotomography. *Structure* **19**, 147-154 (2011).

42. Murphy, G. E. *et al*. Correlative 3D imaging of whole mammalian cells with light and electron microscopy. *J. Struct. Biol.* **176**, 268-278 (2011).

43. Risco, C. *et al*. Specific, sensitive, high-resolution detection of protein molecules in eukaryotic cells using metal-tagging transmission electron microscopy. *Structure* **20**, 759-766 (2012).

44. Gaudin, R. *et al*. Dynamics of HIV-containing compartments in macrophages reveal sequestration of virions and transient surface connections. *PLoS One* **8**, e69450 (2013).

45. Desdouits, M. *et al*. Productive infection of human skeletal muscle cells by pandemic and seasonal influenza A(H1N1) viruses. *PLoS One* **8**, e79628 (2013).

46. Ligeon, L. A. *et al*. Role of VAMP3 and VAMP7 in the commitment of Yersinia pseudotuberculosis to LC3-associated pathways involving single- or double-membrane vacuoles. *Autophagy* **10**, 1588-1602 (2014).

47. Fenaroli, F. *et al*. Nanoparticles as Drug Delivery System against Tuberculosis in Zebrafish Embryos: Direct Visualization and Treatment. *ACS Nano* **8**, 7014-7026 (2014).

48. Resa-Infante, P. *et al*. Importin-alpha7 is required for enhanced influenza A virus replication in the alveolar epithelium and severe lung damage in mice. *J. Virol.* **88**, 8166-8179 (2014).

49. Müller-Reichert, T. & Verkade, P. Methods in Cell Biology - Correlative Light and Electron Microscopy 1st edn. Vol. 111 (eds. Müller-Reichert, T.;Verkade, P.), 1-445 (Elsevier, 2012).

50. Müller-Reichert, T. & Verkade, P. Methods in Cell Biology - Correlative Light and Electron Microscopy II 1st edn. Vol. 124 (eds. Müller-Reichert, T.;Verkade, P.), 1-442 (Elsevier, 2014).

51. Kuo, J. Electron Microscopy: Methods and Protocols, Methods in Molecular Biology, 3rd edn. Vol. 1117 (ed. Kuo J.), DOI: 10.1007/978-1-62703-776-1 (Humana Press, 2014).